COMMUNICATIONS IN SCIENCE AND TECHNOLOGY
Homepage: cst.kipmi.or.id

Integrated GEE–ERT–XRF framework for detecting in-situ rare oxide formation in tropical lowland clays

Uyu Saismana[a,b], Agus Mirwan[c,*], Sunardi[d] , Suryajaya[e], Doni Rahmat Wicakso[c]

[a]*Department of Geological Engineering, Lambung Mangkurat University, Banjarbaru 70714, Indonesia*
[b]*Environmental Science Doctoral Program, Lambung Mangkurat University, Banjarmasin 70123, Indonesia*
[c]*Department of Chemical Engineering, Lambung Mangkurat University, Banjarbaru 70714, Indonesia*
[d]*Department of Chemistry, Lambung Mangkurat University, Banjarbaru 70714, Indonesia*
[e]*Department of Physics, Lambung Mangkurat University, Banjarbaru 70714, Indonesia.*

Article history:
Received: 12 January 2026 / Received in revised form: 5 May 2026 / Accepted: 31 May 2026

Abstract

Understanding in-situ rare oxide formation in tropical lowlands remains challenging due to the extensive peat–clay cover and the limited surface accessibility. This study presents a reproducible integrated workflow combining cloud-based hydrographic analysis in Google Earth Engine (GEE), two-dimensional electrical resistivity tomography (ERT), and X-ray fluorescence (XRF) geochemistry to investigate rare oxide occurrence in South Kalimantan, Indonesia. MERIT Hydro data that had been processed within the GEE framework were utilized for the delineation of buried palaeochannel traces. This was followed by ERT profiling and core drilling to characterize the subsurface lithology. XRF analyses indicate Yb_2O_3 concentrations of 0.01–0.04 wt% and Re_2O_7 of 0.00–0.08 wt% within clay layers at approximately 3–4 m depth. The results of spatial correlation analysis demonstrate weak relationships between oxide distribution and palaeochannel proximity ($|r| < 0.3$) but strong positive relationship between resistivity and oxide concentrations ($r > 0.75$). The results obtained lend significant support to an in-situ formation model, primarily controlled by lithological and geochemical processes as opposed to fluvial transport. The proposed GEE–ERT–XRF workflow offers a preliminary operational framework for detecting subtle, clay-hosted rare oxide signatures in data-limited tropical lowland environments. The findings demonstrate that efficacy of subsurface resistivity as a proxy for identifying geochemical trapping horizons associated with rare oxide enrichment beneath peat–clay cover. The proposed workflow further provides a cost-effective, scalable, and reproducible approach for early-stage mineral exploration and subsurface resource screening in tropical lowland regions where conventional geological mapping is limited by poor surface exposure.

Keywords: Google earth engine; electrical resistivity tomography; X-ray fluorescence; in-situ rare oxide formation; tropical lowland clays

1. Introduction

Understanding subsurface mineral formation in tropical lowland environments remains challenging due to the presence of extensive peat–clay cover, dense vegetation, and limited surface exposure. These conditions restrict conventional geological mapping and hinder the detection of subtle mineralization processes occurring beneath low-relief terrains. As a consequence, distinguishing between in-situ geochemical formation and fluvial redistribution of rare oxides requires integrated analytical approaches that extend beyond surface-based observations.

Ancient buried river systems, also known as palaeochannels, are commonly interpreted as potential pathways for sediment and metal transport in lowland basins. Previous studies have demonstrated that palaeochannel mapping provides valuable insights into landscape evolution, sedimentary architecture, and subsurface resource distribution when combined with remote sensing and geophysical methods [1–3]. However, most documented applications are concentrated in arid or semi-arid regions where geomorphic signatures remain relatively well preserved [1,4]. In humid tropical environments, where palaeochannels are obscured by thick peats and fine-grained sediments, their influence on subsurface geochemical processes remains poorly constrained.

Recent advances in cloud-based geospatial platforms, particularly Google Earth Engine (GEE), have enabled large-scale hydrographic and geomorphological analysis using global datasets [4,5]. Concurrently, near-surface geophysical methods such as electrical resistivity tomography (ERT) have been shown to be effective tools for resolving subsurface lithological variations in lowland settings [6,7]. Furthermore, laboratory geochemical techniques such as X-ray fluorescence (XRF) allow for quantitative assessment of elemental and

* Corresponding author.
Email: agusmirwan@ulm.ac.id
https://doi.org/10.21924/cst.11.1.2026.1883

oxide composition. Despite the individual strengths of these approaches, they are rarely integrated into a single, reproducible workflow designed for subsurface assessment in tropical lowland environments, particularly within applied science and technology contexts [4,5,8].

Rare earth elements and the associated rare oxides have attracted mounting interest in view of their strategic importance for advanced technologies and clean-energy applications [9–11]. In tropical weathering environments, the mobility, fractionation, and retention of these elements are found to be strongly determined by lithology, clay mineralogy, and redox dynamics [12–14]. Clay-rich horizons dominated by smectite and kaolinite are widely recognized as effective geochemical traps that promote ion adsorption and localized oxide stabilization [15,16]. Nevertheless, the extent to which such processes operate independently of palaeofluvial transport in tropical lowland systems has not been systematically evaluated using integrated, multi-scale datasets. In contrast to previous studies that implemented these techniques independently, this study proposes a reproducible and field-validated integration strategy specifically designed for peat–clay tropical systems, with an emphasis on the predictive linkage between resistivity-derived lithological domains and rare oxide enrichment.

This study addresses this gap by applying an integrated GEE–ERT–XRF framework to investigate the spatial relationship between buried palaeochannels, subsurface lithology, and rare oxide occurrence in the tropical lowlands of South Kalimantan, Indonesia. This research combines cloud-based hydrographic analysis [5,17], geophysical imaging [6], and laboratory geochemistry [9,15], with the aims of (i) assessing whether rare oxide enrichment is spatially associated with palaeochannel structures and (ii) evaluating the dominant lithological and geochemical controls governing in-situ rare oxide formation beneath peat–clay cover. The proposed workflow offers an operational and transferable approach for subsurface mineral screening in data-limited tropical environments. This study makes a significant contribution to the refinement of conceptual models of rare oxide formation in tropical lowland systems by demonstrating the lithology-dominated enrichment independent of palaeofluvial controls.

2. Materials and Methods

2.1. Study area

The study area is in Sungai Tabuk Subdistrict, Banjar Regency, South Kalimantan, Indonesia (3°23′0.82″–3°23′59.88″ S; 114°42′9.72″–114°42′22.98″ E). The region is characterized by low-lying tropical plain (with a topography of less than 15 meters above sea level) that is predominantly composed of peat–clay deposits. Geologically, the area comprises the Pliocene–Pleistocene Dahor Formation overlain by Holocene alluvial sediments [18–20]. The Dahor Formation is composed mainly of quartz sandstone, conglomerate, claystone, and minor lignite, indicating a potential source for rare metal-bearing minerals subjected to intense tropical weathering.

2.2. Hydrographic analysis using Google Earth Engine

The delineation of buried palaeochannel networks was facilitated by the utilization of the MERIT Hydro Global Hydrography Dataset [17], which was processed within the GEE cloud platform. MERIT Hydro provides global flow direction and flow accumulation layers at approximately 90 m spatial resolution. The data processing was conducted using JavaScript-based scripting in GEE following established hydrographic extraction procedures [4,5]. A flow accumulation threshold exceeding 5,000 pixels was applied to identify major buried drainage pathways beneath vegetated and fine-grained surfaces. The extracted palaeochannel features were cross-checked against Sentinel-2 imagery (10 m resolution) and hydrographic vector data from the Indonesian Geospatial Information Agency to ensure spatial consistency. The generation of outputs at multiple cartographic scales (1:150,000–1:500,000) was undertaken to evaluate spatial relationships with borehole locations. The threshold of 5,000 pixels was selected based on sensitivity testing and previous hydrographic extraction studies in low-gradient terrains, thereby ensuring that only major drainage pathways were captured, while minimizing noise from minor surface depressions.

2.3. Electrical resistivity tomography (ERT)

Subsurface lithological characterization was performed using two-dimensional electrical resistivity tomography (ERT). The measurements were acquired along three profiles, each 120 meters in length, utilizing an ABEM Terrameter LS 2 system with a Wenner–Schlumberger electrode configuration, selected for its balanced sensitivity to vertical and lateral resistivity variations [6]. Electrode spacing was set at 5 m, yielding an investigation depth of approximately 20–25 m. Raw resistivity data were inverted using Res2DInv software employing a least-squares inversion scheme until root-mean-square (RMS) errors were below 5%. The interpretation of resistivity ranges was informed by established tropical lowland references [6,7]. The selection of three ERT profiles was designed to balance spatial coverage and logistical feasibility, ensuring representation across palaeochannel-proximal and distal zones.

2.4. Core drilling and XRF analysis

To validate geophysical interpretations, ten full-core boreholes were drilled to depths of up to 5 m. Core samples were preserved in sealed PVC tubes to maintain natural moisture conditions. Samples of clay were subjected to oven-dried at temperature of 60°C, pulverized to a size of less than 75 μm, and analyzed using a PANalytical Axios mAX 4 kW X-ray fluorescence (XRF) spectrometer. The quantification of major, minor, and trace oxides was conducted, with the analysis encompassing Yb_2O_3 and Re_2O_7. Each sample was analyzed in triplicate, and mean values were used for interpretation to ensure analytical reproducibility [9]. The borehole number (n=10) represents a targeted sampling strategy aimed at validating geophysical interpretations rather than achieving statistical representativeness.

2.5. Spatial integration and statistical analysis

The oxide concentration data were spatially interpolated using inverse distance weighting (IDW) in ArcGIS Pro 3.2, following standard geochemical mapping procedures [21]. All datasets were projected to UTM Zone 50S (WGS84). Spatial overlay analyses were conducted to compare palaeochannel proximity, resistivity values, and oxide distribution. Pearson correlation analysis was applied to quantify relationships between resistivity and oxide concentration as well as between palaeochannel distance and oxide occurrence. Standard spreadsheet-based statistical functions were utilized for the execution of statistical calculations, with correlation coefficients interpreted in accordance with conventional significance thresholds.

3. Results and Discussion

3.1. Hydrographic and palaeochannel mapping

The implementation of hydrographic processing in Google Earth Engine resulted in the delineation of both active and buried drainage features across the designated study area. The outputs of flow accumulation and drainage density outputs derived from the MERIT Hydro dataset reveal a northeast–southwest-oriented palaeochannel network beneath the peat–clay surface (Fig. 1). The extracted paleochannel traces demonstrated spatial continuity and geometric coherence across multiple cartographic scales ranging from 1:150,000 to 1:500,000 (Fig. 2). Spatial comparison with Sentinel-2 imagery and national hydrographic datasets confirms the positional consistency of the reconstructed drainage patterns. The distribution of borehole locations across both paleochannel-proximal and paleochannel-distal zones, enabled the evaluation of spatial relationships with subsurface geochemical data.

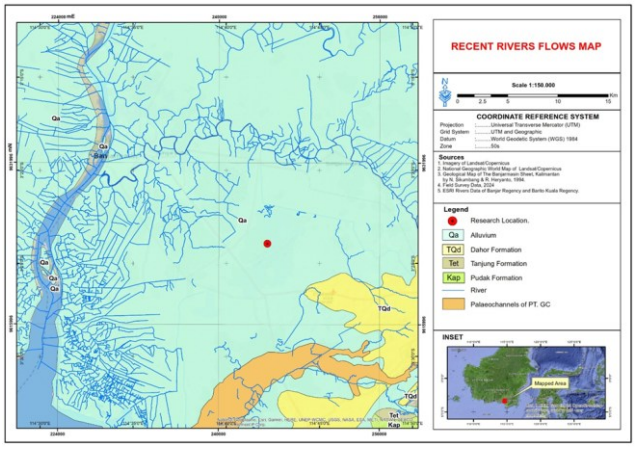

Fig. 1. Recent river flows map

3.2. Subsurface resistivity structure

Two-dimensional ERT profiles have been shown to consistently resolve a vertically layered subsurface structure across all survey lines (Fig. 3). The uppermost unit is characterized by very low resistivity values (<10 Ω·m), followed by layers with resistivity ranges of 10–20 Ω·m and 30–200 Ω·m. A laterally continuous horizon with moderate resistivity values (20–50 Ω·m) is observed at depths of approximately 3–4 m across the profiles. It is notable that beneath this unit, high-resistivity zones (>200 Ω·m) are present. All inversion models achieved root-mean-square (RMS) errors of less than 5%, indicating the attainment of stable and reliable resistivity solutions.

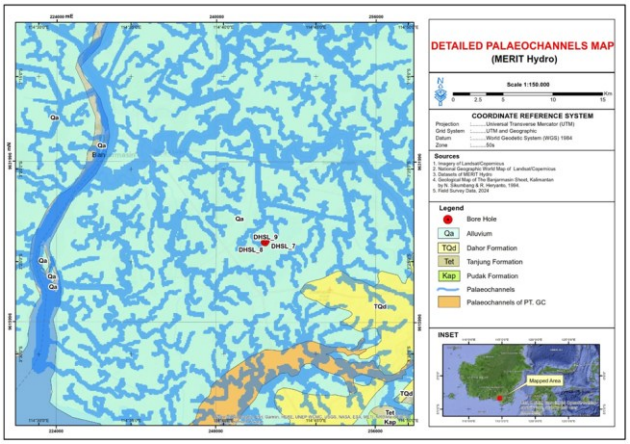

Fig. 2. Detailed palaeochannels map

3.3. Core lithology and geochemical composition

Core drilling results have been found to corroborate the subsurface stratigraphy inferred from the ERT profiles. A dominant clay-rich horizon is observed to occur consistently between 3 and 4 m depth, as illustrated in the representative borehole logs (Fig. 4 and 5). The XRF analysis of clay samples indicates that major oxide compositions are dominated by SiO_2 and Al_2O_3, with minor contributions from Fe_2O_3 and TiO_2 (see Table 1). The presence of trace rare oxides within this horizon has been identified, with Yb_2O_3 concentrations ranging from 0.01 to 0.04 wt% and Re_2O_7 concentrations ranging from below detection to 0.08 wt%. Elevated oxide concentrations are consistently associated with samples collected from the clay horizon, identified by moderate resistivity values.

3.4. Spatial distribution and correlation analysis

Spatial interpolation maps illustrate the heterogeneous distribution of Yb_2O_3 and Re_2O_7 across the study area (Fig. 6 and 7). Pearson correlation analysis reveals weak relationships between palaeochannel proximity and oxide concentrations ($|r| < 0.3$). In contrast, strong positive correlations are observed between clay-layer resistivity values and oxide concentrations, with correlation coefficients exceeding 0.75 for both Yb_2O_3 and Re_2O_7. The statistical relationships presented above are consistent across borehole locations and ERT profiles. Point-based coordinates and oxide concentrations that have been utilized for spatial interpolation and correlation analysis are outlined in Table 2. While Pearson correlation provides a first-order assessment of spatial relationships, more advanced statistical or machine learning approaches may further enhance predictive capability, a subject that will be explored in future work.

Depth (m)	ρ (W.m)	Lithology
1	1.31	Peat
2	2.90	
3	4.73	Peat Sand
4	5.65	Silica Sand
5	1.76	Clay
6	7.78	Silica Sand
7	3.55	
8	4.54	
9	20.49	Gravelly Sand
10	7.62	Silica Sand
12	21.16	Gravelly Sand
16	3.05	Silica Sand
20	30.46	Gravelly Sand

Fig. 3. Two-dimensional ERT profile showing layered resistivity structure and the moderate-resistivity clay horizon at ~3–4 m depth associated with rare

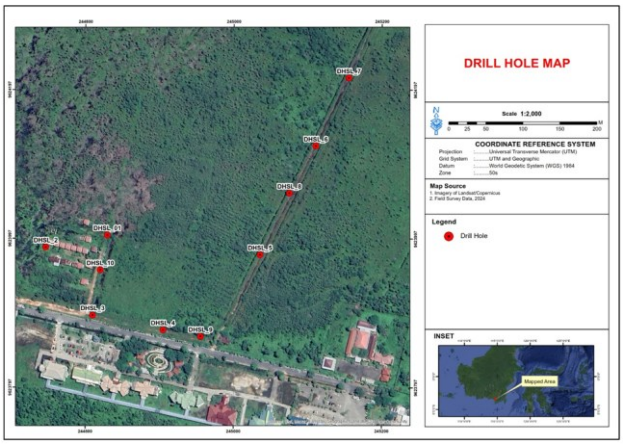

Fig. 4. Spatial distribution of borehole locations relative to reconstructed palaeochannel networks in the study area

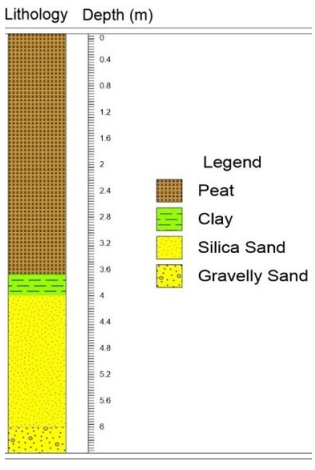

Fig. 5. Log bore (E680)

3.5. Mechanistic controls on rare oxide occurrence

The results demonstrate that the spatial distribution of rare oxides is not significantly associated with palaeochannel geometry, despite the clear delineation of buried drainage systems (Fig. 1 and 2). This weak geomorphic–geochemical coupling indicates that palaeofluvial transport is not the dominant mechanism governing rare oxide occurrence in the study area. Instead, the strong correlation between oxide enrichment and the moderate-resistivity clay horizon (see Fig. 3; Fig. 6–7) suggests that mineralization is primarily controlled by in-situ lithological and geochemical processes. A similar decoupling between geomorphic structures and geochemical anomalies has been reported in tropical lowland and regolith-hosted systems, where post-depositional processes dominate elemental redistribution [12,16,22].

Table 1. Mass composition of drill hole data

Compound	Mass compositions (%)					
	E680	E683	E687	E690	E692	E695
Al_2O_3	23.3	17	17.8	15	16	19.7
SiO_2	63.6	71.3	72.1	45.7	75.3	69.4
Na_2O	0.001	0.003	0.002	0.003	0.001	0.002
MgO	0.002	0.001	0.003	0.001	0.002	0.001
SO_3				11		
P_2O_5		0.96				0.74
K_2O	0.32	0.13	0.12	1.1	0.092	0.14
CaO	0.39	0.39	0.35	0.35	0.33	0.36
TiO_2	5.66	5.46	5.77	2.65	4.75	5.19
V_2O_5	0.11	0.062	0.062	0.081	0.049	0.061
Cr_2O_3	1.27	1.32	0.879	0.2	0.981	1.15
MnO	0.042	0.039	0.029	0.13	0.027	0.032
Fe_2O_3	4.37	2.45	2.03	19.9	1.73	2.38
NiO	0.052	0.043	0.03	0.066	0.021	0.034
CuO	0.049	0.042	0.039	0.072	0.035	0.039
ZnO	0.01	0.007		0.02		0.005
MoO_3				3.5		
ZrO_2	0.61	0.62	0.52		0.55	0.55
Yb_2O_3	0.02	0.01	0.04	0.04	0.04	0.02
Re_2O_7	0.07	0.08		0.08		0.06
LoI	0.06	0.08	0.14	0.07	0.04	0.11

Table 2. Spatial coordinates and concentrations of Yb_2O_3 and Re_2O_7 used for interpolation and correlation analysis

No	Sample ID	Drill Hole	Longitude (°E)	Latitude (°S)	Yb_2O_3 (wt%)	Re_2O_7 (wt%)
1	DHSL_1	E680	114.7034	3.3990	0.02	0.07
2	DHSL_2	E682	114.7027	3.3991	0.00	0.00
3	DHSL_3	E683	114.7033	3.3999	0.01	0.08
4	DHSL_4	E685	114.7041	3.3835	0.00	0.00
5	DHSL_5	E687	114.7053	3.3992	0.04	0.00
6	DHSL_6	E689	114.7059	3.3980	0.00	0.00
7	DHSL_7	E690	114.7064	3.3971	0.04	0.08
8	DHSL_8	E692	114.7057	3.3985	0.04	0.00
9	DHSL_9	E694	114.7046	3.3836	0.00	0.00
10	DHSL_10	E695	114.7034	3.3994	0.02	0.06

The clay horizon, identified at a depth of approximately 3–4

meters, functions as a low-permeability geochemical domain capable of retaining dissolved metal species. In humid tropical environments, smectite- and kaolinite-rich clays promote ion adsorption through surface complexation and cation exchange mechanisms [15,23]. The moderate resistivity values (20–50 Ω·m) observed in this horizon are consistent with partially saturated clay layers experiencing periodic redox fluctuations, conditions known to enhance metal fixation and oxide stabilization [6,7]. This decoupling suggests that post-depositional geochemical processes, including adsorption–desorption cycles and redox-driven precipitation, exert stronger control over rare oxide localization than primary sediment transport mechanisms. This behavior is consistent with tropical regolith systems where chemical weathering and groundwater fluctuations dominate elemental redistribution rather than fluvial processes.

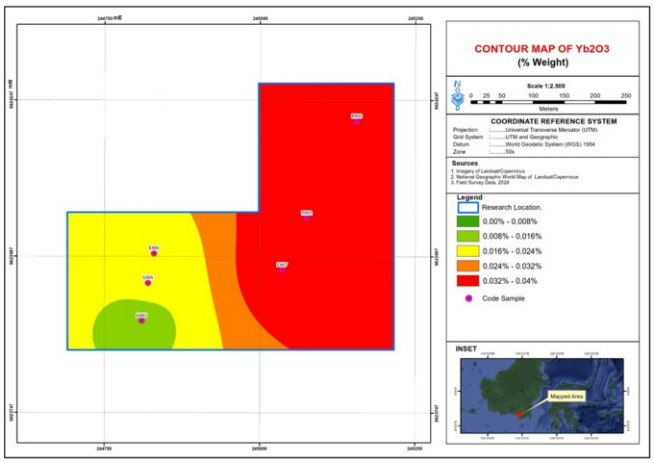

Fig. 6. Spatial distribution of Yb_2O_3 concentrations in the study area derived from IDW interpolation of borehole data

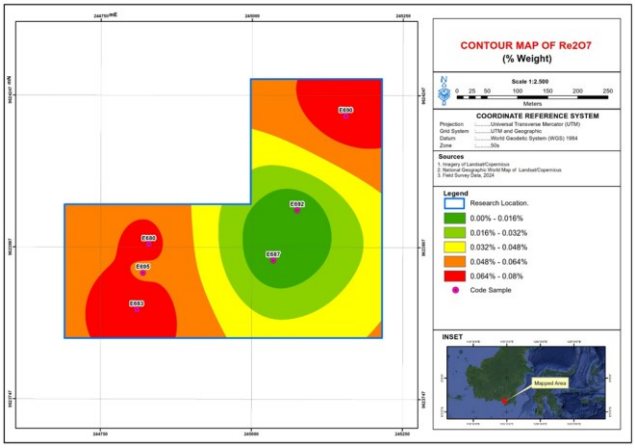

Fig. 7. Spatial distribution of Re_2O_7 concentrations in the study area derived from IDW interpolation of borehole data

3.6. Source materials and in-situ formation processes

The geochemical characteristics of the clay horizon indicate that Yb and Re were derived from the weathering of quartzitic and molybdenite-bearing lithologies of the Dahor Formation. Oxidative weathering of REE- and sulfide-bearing minerals releases mobile metal species that migrate over limited vertical distances before being immobilized within clay-rich horizons [12,15]. In lowland tropical systems, fluctuating groundwater levels further promote adsorption–desorption cycles, leading to localized enrichment within specific depth intervals rather than widespread lateral dispersion [16,23].

The confinement of Yb_2O_3 and Re_2O_7 enrichment to a narrow depth range (Fig. 4–5; Table 1) supports an in-situ formation model rather than detrital accumulation along palaeochannel pathways. Comparable depth-controlled enrichment has been documented in ion-adsorption-type rare earth deposits formed under intense tropical weathering conditions, where heavy rare earth elements have been observed to preferentially accumulate within specific clay horizons [15,22]. This behaviour is in contrast to that observed in fluvially controlled enrichment models reported in semi-arid systems, thus highlighting a distinct geochemical regime in humid tropical settings.

3.7. Implications for integrated exploration workflows

From a technological standpoint, the results demonstrate that palaeochannel mapping alone is insufficient for predicting rare oxide occurrence in tropical lowland environments. Despite the efficacy of cloud-based hydrographic analysis in the reconstruction of buried drainage systems at regional scales (Fig. 1–2) [4,5], these features do not reliably indicate subsurface geochemical enrichment. Instead, the integration of geophysical indicators—specifically moderate-resistivity clay horizons identified by ERT (Fig. 3)—with targeted geochemical validation provides a more robust screening strategy.

The strong correlation between resistivity and oxide concentration (Fig. 6–7) highlights the utility of ERT as a proxy for identifying geochemical trapping horizons beneath peat–clay cover. When combined with GEE-based spatial analysis and laboratory XRF measurements, the proposed GEE–ERT–XRF workflow constitutes a scalable and reproducible framework for subsurface mineral screening in data-limited tropical environments. It has been posited that similar integrated, multi-sensor approaches should be considered for exploration in deeply weathered and regolith-hosted systems, where surface indicators are minimal or absent [24,25]. The present study's emphasis on methodological integration and workflow reproducibility aligns with recent contribution of applied science, as documented in Communications in Science and Technology. These contributions highlight the significance of transferable and operational analytical frameworks for environmental and subsurface characterization [26].

3.8. Broader applicability and methodological limitations

While the present study focuses on Yb_2O_3 and Re_2O_7 in South Kalimantan, it is argued that the integrated workflow can be transferred to other tropical lowland systems characterized by thick sedimentary cover and restricted surface exposure. The approach is particularly suitable for early-stage exploration and environmental screening where non-invasive and reproducible methods are required. However, it is

important to note that the workflow does not substitute for detailed mineralogical, isotopic, or metallurgical analyses, which remain necessary for definitive genetic classification and resource assessment. The spatial representativeness of the results is constrained by the limited number of boreholes and the shallow investigation depth; therefore, conclusions should be interpreted as site-specific rather than universally applicable. It is important that future studies incorporating deeper drilling, larger spatial coverage, and multi-scale datasets are conducted to validate the scalability of the proposed framework.

4. Conclusion

The present study demonstrates that rare oxide enrichment in tropical lowland clays is governed primarily by in-situ lithological and geochemical controls rather than palaeofluvial transport. Integration of Google Earth Engine–based hydrographic analysis, electrical resistivity tomography, and X-ray fluorescence geochemistry reveals that Yb_2O_3 and Re_2O_7 are concentrated within a moderate-resistivity clay horizon at approximately 3–4 m depth, acting as an effective geochemical trap under fluctuating redox conditions. The weak spatial association with paleochannel networks is in contrast to the strong correlation between oxide concentration and resistivity, thus confirming a lithochemically controlled formation mechanism. Beyond site-specific findings, the proposed GEE–ERT–XRF workflow provides a preliminary operational and scalable framework for screening subtle, clay-hosted mineralization beneath peat and alluvial cover. This offers practical value for mineral exploration and subsurface characterization in data-limited tropical environments. From an applied perspective, the workflow provides a cost-effective early-stage exploration tool for identifying clay-hosted rare oxide targets in environments where data is limited.

Acknowledgements

This research was supported by the Lambung Mangkurat University Research Grant (2024) under Grant No. 1374.7/UN8.2/PG/2024. The authors gratefully acknowledge the Faculty of Engineering and the Graduate Program of Environmental Science, Lambung Mangkurat University, for their invaluable contribution to this research, specifically the provision of laboratory facilities and technical support. Appreciation is also extended to the Geochemical Laboratory and Geophysical Survey teams for their assistance in field data acquisition, core drilling, and analytical measurements. The authors express their gratitude to the Center for Geospatial Information for facilitating access to the hydrographic and spatial datasets. The availability of open-access data from the MERIT Hydro and Sentinel-2 platforms is also acknowledged, which enabled the integrated geospatial analysis conducted in this study.

References

1. R.K. Upadhyay, N. Kishore, M. Sharma, *Delineation and mapping of palaeochannels using remote sensing, geophysical, and sedimentological techniques: A comprehensive approach*, Water Sci., 35 (2021) 100–108.
2. S. Chaudhary, A. Chandra Pandey, B.R. Parida, *Geoinformatics based detection and delineation of paleochannels in hard rock terrain of Koel River Basin, Jharkhand, eastern India*, Groundw. Sustain. Dev., 19 (2022) 100832.
3. H.A. Orengo, C.A. Petrie, *Large-Scale, Multi-Temporal Remote Sensing of Palaeo-River Networks: A Case Study from Northwest India and its Implications for the Indus Civilisation*, Remote Sens., 9 (2017) 735.
4. T. Ullmann, E. Möller, R. Baumhauer, E. Lange-Athinodorou, J. Meister, *A new Google Earth Engine tool for spaceborne detection of buried palaeogeographical features – examples from the Nile Delta (Egypt)*, E&G Quat. Sci. J., 71 (2022) 243–247.
5. R.J. Boothroyd, R.D. Williams, T.B. Hoey, B. Barrett, O.A. Prasojo, *Applications of Google Earth Engine in fluvial geomorphology for detecting river channel change*, WIREs Water, 8 (2021) e21496.
6. S. Uhlemann, O. Kuras, L.A. Richards, E. Naden, D.A. Polya, *Electrical resistivity tomography determines the spatial distribution of clay layer thickness and aquifer vulnerability, Kandal Province, Cambodia*, J. Asian Earth Sci., 147 (2017) 402–414.
7. J.O. Alao, *Determination of the geophysical signature of soft-clay and hard lateritic soils and the implications on geotechnical works using electrical resistivity imaging*, Results Earth Sci., 2 (2024) 100025.
8. M.H. Ridha, Y.F. Arifin, A.S. Abdi, *Optimizing ground control points for UAV photogrammetry: A case study in slope stability mapping*, Commun. Sci. Technol., 10 (2025) 170–178.
9. V. Balaram, Rare earth elements: *A review of applications, occurrence, exploration, analysis, recycling, and environmental impact*, Geosci. Front., 10 (2019) 1285–1303.
10. P. Granvik, J. Hanski, S. Lähdesmäki, A. Jokilaakso, E. Huttunen-Saarivirta, *Critical raw materials for green transition: Key parameters and feasibility index for sufficiency*, Resour. Conserv. Recycl., 218 (2025) 108197.
11. J. Ren, A. Gu, K. Sun, H. Zhang, J. Li, H. Sun, Y. Lu, X. Tong, X. Wu, Z. Zhou, *A Review of Rare Earth Elements Resources in Africa*, Minerals 15 (2025) 980.
12. N. Su, S. Yang, Y. Guo, W. Yue, X. Wang, P. Yin, X. Huang, *Revisit of rare earth element fractionation during chemical weathering and river sediment transport*, Geochem. Geophys. Geosyst., 18 (2017) 935–955.
13. T. Lan, L. Hao, J. Lu, Y. Yin, X. Chen, Y. Fan, W. Zhao, Y. Hou, *Geochemical Behavior of Different Chemical Elements during Weathering of the Basalts in Changbai Mountain, Northeast China*, Sustainability 13 (2021) 12796.
14. H.-J. Han, J.-U. Lee, S.-W. Ji, D.-W. Cho, G.-J. Yim, *Geochemical Behavior of Rare Earth Elements and Their Use as Environmental Indicators*, J. Korean Soc. Miner. Energy Resour. Eng., 62 (2025) 492–506. https://doi.org/10.32390/ksmer.2025.62.4.492.
15. Y. Huang, H. He, X. Liang, Z. Bao, W. Tan, L. Ma, J. Zhu, J. Huang, H. Wang, *Characteristics and genesis of ion adsorption type REE deposits in the weathering crusts of metamorphic rocks in Ningdu, Ganzhou, China*, Ore Geol. Rev., 135 (2021) 104173.
16. M.D. Cascante, C.-Y. Wu, Z.-Y. Hseu, *Fractionation of rare earth elements in tropical soils from marine mudstone along a toposequence*, Heliyon 11 (2025) e42097.
17. D. Yamazaki, D. Ikeshima, J. Sosa, P.D. Bates, G.H. Allen, T.M. Pavelsky, *MERIT Hydro: A High-Resolution Global Hydrography Map Based on Latest Topography Dataset*, Water Resour. Res., 55 (2019) 5053–5073.
18. K. Sikumbang, R. Heryanto, *Peta Geologi Lembar Banjarmasin, Kalimantan 1:250,000 = Geological Map of the Banjarmasin Sheet,*

Kalimantan, Pusat Penelitian dan Pengembangan Geologi, Bandung, Indonesia, 1994.

19. A. Mirwan, S. Susianto, A. Altway, R. Handogo, *Kinetic model for identifying the rate controlling step of the aluminum leaching from peat clay*, J. Teknol., 80 (2018).
20. A. Mirwan, S. Susianto, A. Altway, R. Handogo, *Temperature-dependent kinetics of aluminum leaching from peat clay*, Malays. J. Fundam. Appl. Sci., 16 (2020) 248–251.
21. J. Mihajlovic, A. Bauriegel, H.-J. Stärk, N. Roßkopf, J. Zeitz, G. Milbert, J. Rinklebe, *Rare earth elements in soil profiles of various ecosystems across Germany*, Appl. Geochem., 102 (2019) 197–217.
22. W. Liu, Y. Li, X. Wang, L. Cui, Z. Zhao, C. Liu, Z. Xu, *Weathering stage and topographic control on rare earth element (REE) behavior: New constraints from a deeply weathered granite hill*, Chem. Geol., 610 (2022) 121066.
23. X. Fu, Z. Yi, W. Fu, J. Liu, Z. Han, G. Fang, X. Sha, X. Liu, C. Xu, *Mineralogy and weathering of REE minerals in the Liuchen granite, Guangxi, southern China: Implications for HREE enrichment in the granite regolith*, Ore Geol. Rev., 169 (2024) 106099.
24. T.G. Bamforth, H.M. Lampinen, L. Lynham, N. Reid, R. Thorne, M. Iglesias-Martínez, J. Brugger, B. Cribb, B. Hazelden, F. Xia, *Unsupervised geochemical characterisation of deeply weathered terrains and regolith-hosted REE deposits: Rationale and benefits for exploration*, Ore Geol. Rev., 181 (2025) 106634.
25. Z. Luo, E. Farahbakhsh, R.D. Müller, R. Zuo, *Multivariate statistical analysis and bespoke deviation network modeling for geochemical anomaly detection of rare earth elements*, Appl. Geochem., 174 (2024) 106146.
26. Y. Rahmawati, K. Woraratpanya, I. Ardiyanto, H.A. Nugroho, *Evaluating the effectiveness of facial actions features for the early detection of driver drowsiness in driving safety monitoring system*, Commun. Sci. Technol., 10 (2025) 179–189.